Leadership in Sustainable Infrastructure
Leadership en Infrastructures Durables

Vancouver, Canada
May 31 – June 3, 2017/ *Mai 31 – Juin 3, 2017*

PREDICTION OF BURST LOAD IN PRESSURIZED PIPELINES USING EXTENDED FINITE ELEMENT METHOD (XFEM)

Agbo, Sylvester[1,6], Lin, Meng[2], Ahmed, Arman[3], Cheng, J.J. Roger[4], and Adeeb, Samer[5]
[1, 2,3,4,5] University of Alberta, Canada
[6] adeeb@ualberta.ca

Abstract: Application of principles of fracture mechanics to response of pipelines with circumferential flaw subjected to varying internal pressure and tensile load is a relatively new field. Many researchers have studied the integrity of pipelines using many methods, but no well-established methodology exists to address the biaxial loading state introduced by a combination of internal pressure and eccentric tensile loading on pipelines. Fracture mechanics principles were applied to pipe specimens with circumferential flaw, subjected to varying internal pressure and eccentric tensile load. Eight full-scale pressurized tests were previously carried out in our laboratory on X52 grade NPS (nominal pipe size) 12 inches steel pipe subjected to eccentric tensile load with pre-machined flaw close to the girth weld. This paper discusses the development of finite element models using the extended finite element method (XFEM) to predict burst load in pipes due to crack growth under the loading conditions of full-scale tests. The model results were validated using the load history obtained during the full-scale tests. The crack mouth opening displacement (CMOD) - load history of each model was analyzed to produce compliance measurements at increasing levels of internal pressure. This paper compares the numerical results including burst load predicted by XFEM models with the results of the full-scale tests. This paper illustrates the potential advantage of XFEM technique, a tool easy to implement, to predict burst load in steel pipelines due to crack growth.

Keywords: burst load, crack growth, extended finite element method, fracture mechanics, full-scale test, and remote strain.

1 Introduction

Oil and gas pipelines that transverse the remote seismically active regions with harsh environments may be subjected to large plastic strains. This could be as a result of increased ground movement caused by continuous freezing and thawing of the ground in addition to continuous variation of internal pressure in the pipes. Moreover, seismic activities, frost heave, and slope instabilities can introduce high plastic deformations to onshore and offshore pipelines. There has been an increasing demand to design pipelines that can withstand these large plastic strains [1]. Presence of fabrication flaws in girth weld are one of the major factors leading to failure in pipelines due to the associated stress concentrations and hence excessive tensile strain within the region [2]. The ability of girth weld with defects (flaw) to resist fracture, limits the tensile strain capacity of pipelines [1]. The presence of flaw in pipe welds coupled with the changes in internal pressure in pipelines subjected to complex environmental and working load, could lead to crack initiation and propagation which eventually could lead to burst (failure). The extended finite element method [3-6] which can timely simulate and record the damage evolution history, has been widely used to model

ductile fracture procedure including crack initiation and propagation. Today, the XFEM is one of the most useful methods in modelling cracks [7].

Previously, Abdulhameed et al [8] conducted full-scale tests on X52 grade NPS 12 steel pipeline in our laboratory to investigate the effect of internal pressure on the tensile strain capacity of the pipeline with different sizes of circumferential flaws. They concluded that the internal pressure effect was responsible for reduction in the tensile strain capacity (TSC) of the pipeline up to 50% and also that the level of internal pressure has no effect on the final CMOD at failure for tests with the same flaw size. This paper is focused on the use of XFEM to model full- scale pressurized tests of X52 pipeline with different levels of internal pressure subjected to eccentric tensile loading to predict the burst load of pressurized pipelines and to validate the usefulness of XFEM as a veritable tool for modelling crack growth. Since the strain capacity is defined as the strain corresponding to maximum load (combined internal pressure and tensile load), the measured TSC will correspond to the failure load which is referred to as burst load in this paper.

2 Methodology

2.1 Full-scale test experiment.

Eight full-scale tests were carried out previously in our laboratory by Abdulhameed et al [8].

Table 1 shows the parameters used in test 7 and 8 of the eight full-scale tests previously conducted, and their models 7 and 8 respectively. The pipe length was 1219.2mm (4 OD) with girth weld in the mid-length of the pipe. A flaw was introduced close to the girth weld using a machined saw cut. The flaw dimensions for test 7 and 8 which were modeled in this paper were length of 150mm with a depth of 50% of the nominal wall thickness (3.4mm) as shown in Table 1.The pipes were tested in a materials testing system (MTS) machine under eccentric tensile displacement in the presence of internal pressure. The eccentricity was to ensure that the circumferential flaw was subjected to the highest tensile strain throughout the test. A cap plate was welded to the pipe ends and connected to an end plate using 14 bolts. A tongue piece was positioned on the end plates with an eccentricity of 50mm to provide the eccentric loading. This tongue plate was fitted into a pin–yoke assembly that connects the pipe to the MTS machine as shown in Figure 1. The internal pressures causing 30% and 80% specified minimum yield stress (SMYS) of hoop stress were 3.487MPa and 11.704MPa respectively, these were obtained using the Barlow's formula [8]. The loading was applied in two steps. In the first step, the internal pressure was applied by filling the pipe with water through an opening located in the bottom end plate. In the second step, while the internal pressure was kept constant, an eccentric tensile displacement was applied to the top tongue through the MTS in increments until the instance of failure. Failure (burst) is defined as the point in time when crack penetrated through the wall thickness of the pipe and water seeps out from the pipe. The strains were evaluated using a Digital Image Correlation (DIC) technique, to obtain the variation of the strain field on the tension side of the pipe during the experiment along the pipe length. Strain gauges were positioned at quarter of the pipe length (0.25L) away from the cap plate at 90-degrees interval around the pipe circumference to record the remote strain. Clinometers were attached to the top and bottom end plates to measure the rotation of the pipe ends caused by the loading eccentricity, throughout the test. The MTS measured and recorded the reaction force and displacement during the test.

Table 1: Tests and XFEM model parameters [8]

Test / Model	Outer diameter (mm)	Pipe length (mm)	Internal pressure (% SMYS)	Internal pressure (MPa)	Flaw depth (mm)	Flaw length (mm)
Test 7	304.8	1219.2	80	11.704	3.4	150
Model 7	304.8	1219.2	80	11.704	3.4	150
Test 8	304.8	1219.2	30	3.387	3.4	150
Model 8	304.8	1219.2	30	3.387	3.4	150

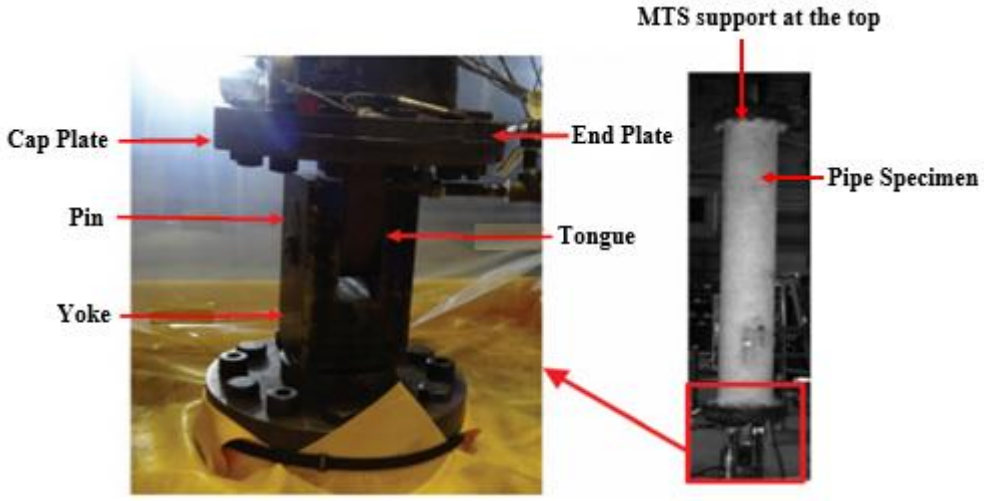

Figure 1: Full-scale test set-up and the details of the loading support. Abdulhameed et al [8]

2.2 XFEM Model

The improvement of XFEM compared to the traditional FEA was due to the introduction of additional functions that made it suitable for modelling stationary discontinuities like crack. These newly introduced functions made modeling of growing cracks much easier since, unlike the traditional FEA, there is no need for re-meshing the crack surface as the crack progresses [9, 10]. Shown in equations (1) and (2) are the nodal enrichment functions that consist of the near-tip asymptotic functions which capture the singularity around the crack tip and the discontinuous function that represents the displacement jump across the crack surfaces. An approximation for a displacement vector function u is given as:

$$[1]\ u = \sum_{I=1}^{N} N_I(x)\left[u_I + H(x)a_I + \sum_{\propto=1}^{4} F_{\propto}(x)b_I^{\propto}\right]$$

Where, $N_I(x)$, are the nodal shape functions, the first term u_I, is the nodal displacement vector; the second terms are the nodal enriched degree of freedom vector a_I, and the associated discontinuous jump function $H(x)$ across the crack surfaces. The third term is the product of the nodal enriched degree of freedom vector $b_I^{\propto}$, and the associated elastic asymptotic crack-tip functions, $F_{\propto}(x)$. From the right-hand side, the first term applies to all the nodes in the model, the second term is only valid for nodes whose shape function support is cut by the crack interior, while the third term is valid only for nodes whose shape function support is cut by the crack tip [11, 12].

The asymptotic crack tip functions in an isotropic elastic material, $F_{\propto}(x)$, is given as:

$$[2]\ F_{\propto}(x) = \left[\sqrt{r}\sin\frac{\theta}{2}, \sqrt{r}\cos\frac{\theta}{2}, \sqrt{r}\sin\theta\sin\frac{\theta}{2}, \sqrt{r}\sin\theta\cos\frac{\theta}{2}\right]$$

Where(r, θ), is a polar coordinate system with its origin at the crack tip and $\theta = 0$ is tangent to the crack at the tip [11].

Two 3D XFEM models of full-scale tests were conducted using ABAQUS software to investigate the behavior of the tested pipes under the effect of internal pressure and eccentric tensile loading. Symmetry was considered in modeling, thus one longitudinal half of the pipe was simulated as shown in Figure 2. The modelling involved creating of parts in accordance with the dimension of the pipe test specimen. The model has an outer diameter (OD) of 12in (304.8 mm), length of 4 OD (1219.2mm), nominal wall thickness of 0.268in (6.8mm), flaw depth of 3.4mm and flaw length of 150mm. Figure 2 is a schematic representation of the assembled pipe model.

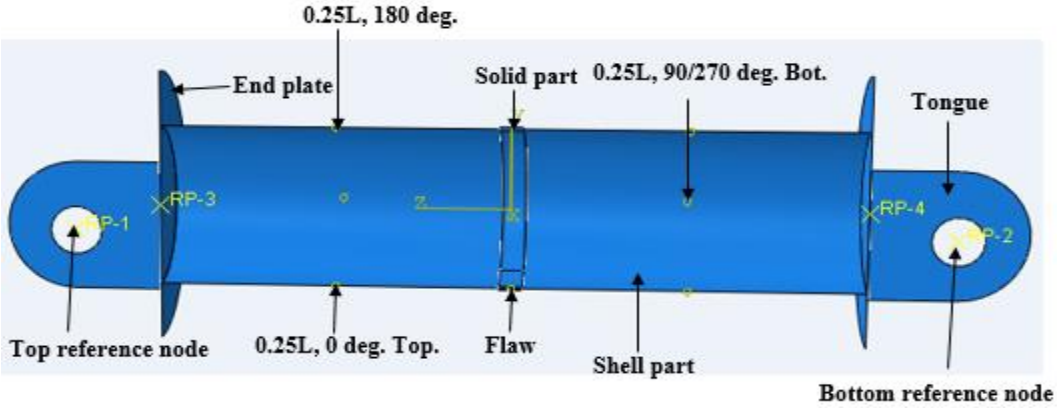

Figure 2: Assembled components of the model showing the geometry and reference points.

A total of eight instances were created which comprised of "solid part", which is a 3D solid part of the pipe model located at the mid-length, it was chosen to be 3D solid to allow for visualization of the crack growth and to create the solid domain for insertion of the flaw. The entire pipe length was not modelled as solid to reduce the number of element mesh created in the model for easy running of the model. Two "shell part" instances were created which were shell extrusion elements that form the rest of the pipe length. Both were connected to the solid part using shell-solid coupling constraint, this created an interaction that made both to function as a single part. Two end plates were modeled as shell planer rigid body elements that represented a combination of the end plate and the cap plate as used in the full-scale test and were connected to shell part using a tie constraint, which simulated the welded joint. Two loading tongues were also modeled as shell planer rigid bodies and connected to the end plates at an eccentricity of 50mm to introduce the eccentric loading in the model using tie constraint. The tongues at both ends of the model form the top and bottom loading reference nodes, and were modeled as rigid bodies. The flaw was modelled as a shell planer element and inserted into the solid part of the model and subsequently created an interaction with the solid domain as XFEM crack. These instances were assembled to form the model geometry shown in Figure 2. An 8-node linear brick element mesh with reduced integration, hourglass control (AC3D8R) was used in the solid part. The mesh size was controlled by the flaw size to ensure good interaction between the flaw and the solid part to stimulate crack growth. Meshes within the flaw vicinity were smaller in size compared to other parts as shown in Figure 3. The shell part was meshed with a 4-node doubly curved thin shell with reduced integration, hourglass control and finite membrane strains. The crack propagation associated with the pipe specimen was assumed to be in Mode-I fracture. The maximum principal stress (σ_{maxps}) and fracture energy (Gc) were selected as the key damage parameters in the XFEM model. There were non-existing values for σ_{maxps} and Gc recommended for X52 grade steel material, but Nonn et al and Scheider et al [13-15] proposed recommended values to be used for three higher grade steel: σ_{maxps} =1375MPa and Gc = 900N/mm for X65 grade steel, σ_{maxps} =1600MPa and Gc = 900N/mm for X80 grade steel and σ_{maxps} =1700MPa and Gc =700N/mm for X100 grade streel.

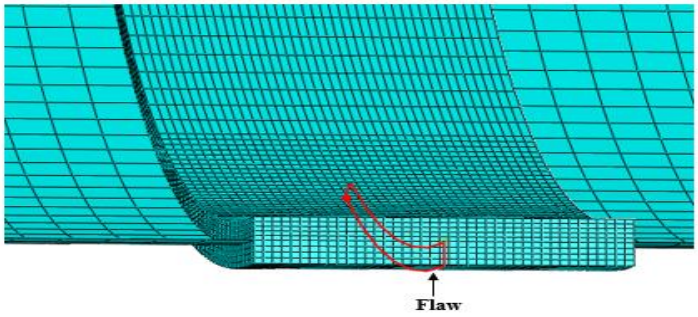

Figure 3: A section of the model showing the mesh sizes and the position of the flaw.

2.3 Materials

The pipes were modelled as a mechanical, elasto-plastic isotropic material with Young's Modulus of 199GPa and Poisson ratio 0.3. The yield stress and plastic strain parameters were obtained from the true stress-plastic strain curve obtained from small scale tension test and Charpy V-notch impact tests carried out on X52 grade pipe material in our laboratory by Lin [16]. The parameters were used as material inputs in the XFEM models. Isotropic strain-hardening plasticity was used to describe the plastic behavior. The maximum principal stress was the damage initiation criterion used in the XFEM model. Energy was selected as the type of damage evolution, while a linear softening with maximum degradation was applied.

A numerical investigation was carried out to identify the most suitable damage parameters σ_{maxps} and *Gc* to use in the XFEM modelling to produce results that agree with the full-scale test experimental result. After series of investigation, σ_{maxps} =700MPa and *Gc* =900N/mm was selected and used in both models.

2.4 Loading and boundary conditions.

An initial condition of symmetry was applied, since the pipe was modelled as a longitudinal half due to symmetry. The bottom tongue was fixed initially while the top was allowed to move in the longitudinal direction only. The pipe was loaded in the XFEM model in two steps. In the first step, the specified internal pressure was applied to the inner surfaces of pipe and end plates while the bottom reference node remained fixed. In the second step, the pipe was subjected to a longitudinal displacement at the top reference node which introduced an eccentric tensile force, and both reference nodes were allowed to rotate about the x-axis. Two models were created; model 7, with 80% SMYS and model 8 with 30% SMYS which represented the full-scale tests 7 and 8 respectively. The model and tests parameters were as shown in Table 1. The remote strain (ε0.25L) is defined as the strain reading at a quarter of the pipe length (L) from the end plates. The position of 0.25L at angles 0, 90,180 and 270 degrees relative to the center of flaw was shown in Figure 2. This location was chosen to be the remote strain measurements as it represented the flat part in a strain profile along the pipe length as described by Abdulhameed et al [8].

3 Results

The reaction force obtained from the model was taken as the applied tensile force. Remote strain values (ε0.25L) were obtained from a quarter length of the pipe measured from the end plate at an angle of 90 degrees from the center of flaw for top and bottom sides. The remote strain ε0.25L, CMOD, and rotation results obtained from the XFEM models were plotted against the applied tensile force. The result obtained from each model was compared with the corresponding full-scale test result to validate the model.

A comparison of the burst load, i.e. the applied tensile force at which the crack penetrated fully the pipe wall thickness, the remote strain, CMOD and rotation obtained from the full-scale test and that obtained from the models showed good agreement.

Figure 4 shows a plot of applied tensile force versus remote strain up to failure for both tests and models.

The burst load and the corresponding remote strain values of the full-scale tests and XFEM models plotted in Figure 4 were compared in Table 2.

CMOD results obtained from both tests and XFEM models were plotted against the applied tensile force up to failure as shown in Figure 5. CMOD-failure is the CMOD corresponding to the burst load, i.e. when the crack fully penetrated the pipe wall thickness as shown in Figure 6.

Critical CMOD is defined as the crack mouth opening at 97% of the burst load [8]. This represents the crack mouth opening at a point of time when the applied load is almost constant while the crack progressed. CMOD-failure obtained from Figure 5 and the critical CMOD for tests and XFEM models were compared in Table 2.

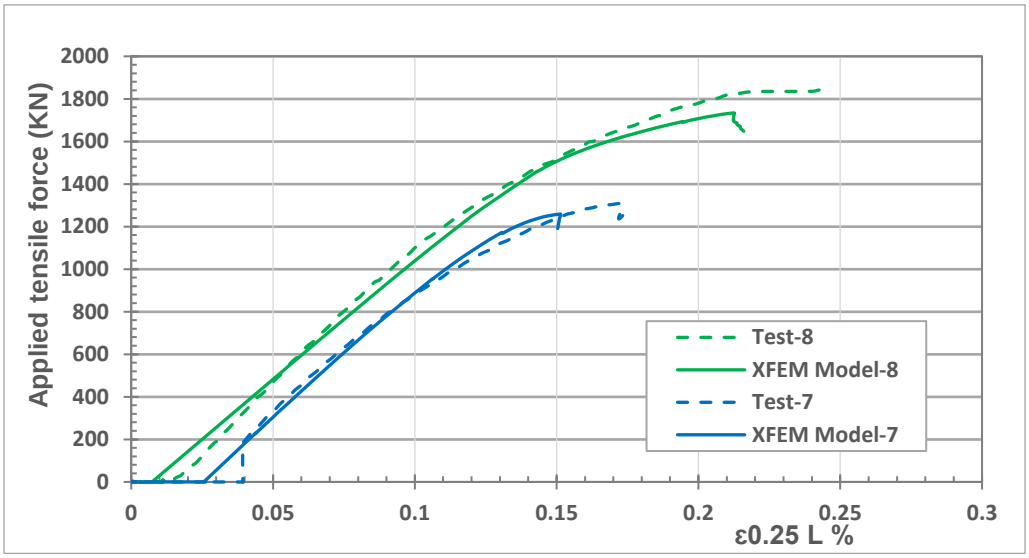

Figure 4: Applied tensile force versus ε0.25L up to failure.

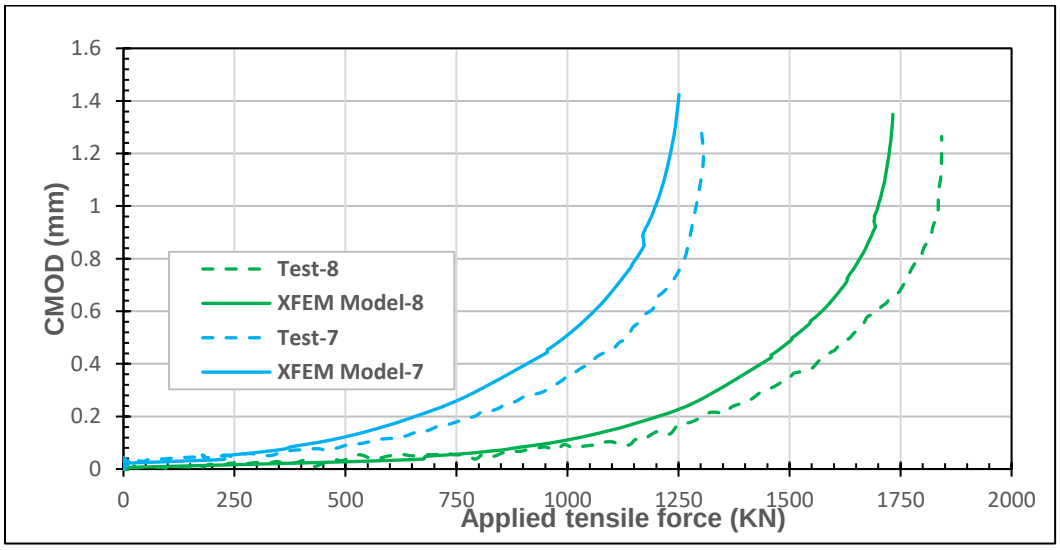

Figure 5: CMOD versus applied tensile force up to failure.

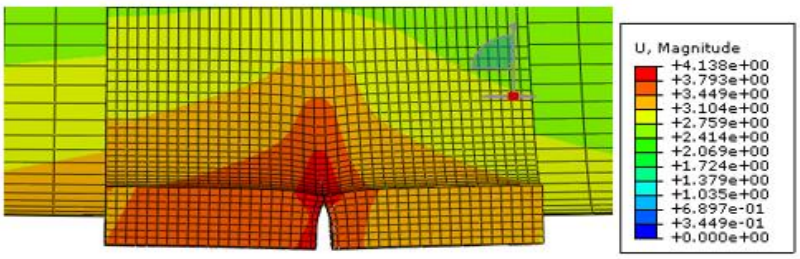

Figure 6: Shows the CMOD of the model at failure.

Similarly, the rotation (degree) of the tests and models due to the eccentric loading was plotted against the applied tensile force up to failure as shown in Figure 7. Rotations at failure from Figure 7, for tests and models were equally compared in Table 2.

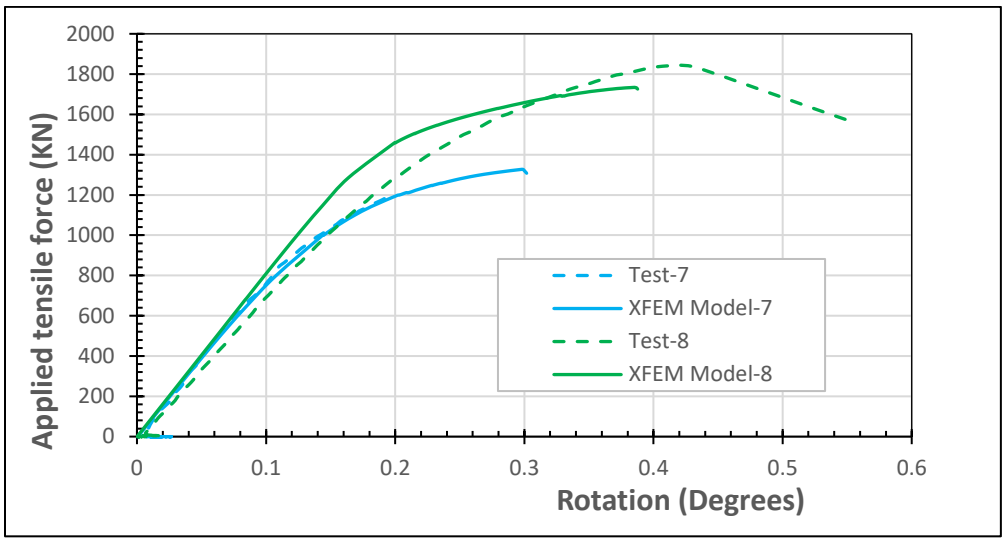

Figure 7: Applied tensile force versus rotation (degree) of the end plate up to failure.

Table 2: Comparison between experimental and XFEM model results.

Model/Test	Internal Pressure (%SMYS)	Burst Load (KN)	ε0.25L (%)	CMOD (mm)	Rotation (Degree)	Critical CMOD (mm)
Test 7	80.0	1302.676	0.1690	1.30	0.23	0.81
Model 7	80.0	1251.170	0.1473	1.42	0.24	0.84
%Difference	0.0	-4.0%	-12.8%	+9.2%	-4.2%	+3.6%
Test 8	30.0	1842.646	0.2428	1.27	0.45	0.81
Model 8	30.0	1734.048	0.2125	1.39	0.40	0.84
%Difference	0.0	-6.0%	-12.5%	+9.4%	-12.5%	+3.6%

Note: "-" / "+" means that, data in Model is lower / higher than data obtained from the full-scale tests.

From Table 2, a comparison of the experimental burst-load and that of the XFEM models showed good agreement, with a percentage difference of -4.0% for XFEM model 7, while XFEM model 8 gave -6.0% difference. The negative sign indicated that the XFEM model gave lower values compared to the experimental test result. When the remote strain was compared, XFEM model 7 gave -12.8% difference while XFEM model 8 gave -12.5%.

Also when the CMOD of the models were compared to that of experiments, XFEM model 7 gave +9.2% while XFEM model 8 gave 9.4% difference. When the rotation was compared, XFEM model 7 gave -4.2% while XFEM model 8 gave -12.5% difference as shown in Table 2. The non-zero rotation at zero tensile force noticed in test 7 was as a result of the high initial internal pressure applied prior to application eccentric tensile force.

3.1 Effect of internal pressure

The burst load, remote strain($\varepsilon 0.25L$) and CMOD obtained from the models with the same flaw size but different internal pressure levels plotted in Figures 4 and 5 were compared in Table 3.

Table 3: Comparison of tests, and the XFEM models due to difference internal pressure level.

Model / Test	Internal pressure (%SMYS)	Burst load (KN)	Remote strain (ε0.25L) %	CMOD (mm)	Critical CMOD (mm)
Test 7	80.0	1302.676	0.1690	1.30	0.81
Test 8	30.0	1842.646	0.2428	1.27	0.81
%Difference	-62.5%	+41.5%	+43.7%	-2.3%	0.0%
Model 7	80.0	1251.170	0.1473	1.42	0.84
Model 8	30.0	1734.048	0.2125	1.39	0.84
%Difference	-62.5%	+39.0%	+44.0%	-2.1%	0.0%

Note: "-" / "+" means that, data in Test/Model 8 is lower / higher than data in the Test/Model 7

When the internal pressure was decreased from 80% SMYS to 30% SMYS, the remote strain at failure increased by 44% while the burst load at failure increased by 39% as shown in Table 3. When the internal pressure increased from 30% SMYS to 80%SMYS, the burst load and remote strain at failure decreased. As the internal pressure increased, there was an increase in both the longitudinal and axial tensile stresses which stimulated early crack growth thus, the pipe failed at a lower applied load.

CMOD results of each model were plotted against the applied load to observe the crack growth during the load increments in the model up to failure as shown in Figure 5. Change in internal pressure did not significantly affect the CMOD-failure since only a difference of -2.1% was obtained. But XFEM models 7 and 8 gave the same critical CMOD value of 0.84mm as shown in Table 3. For the two tests with the same crack dimensions but with different level of internal pressures, the resulting CMOD was found to be very close, with a percentage difference of -2.3%, but both have the same critical CMOD value of 0.81mm as shown in Table 3. This shows that the internal pressure has no effect on the critical CMOD at failure, but model 7 with 80% SMYS internal pressure reached the critical CMOD at lower burst load compared to XFEM model 8 with 30% SMYS internal pressure. It was observed from the curves that lower internal pressure required more load to reach the burst load. Thus, higher internal pressure pipes possess lower burst load and are more susceptible to failure.

3.2 Discussion

Numerical investigation to identify the most suitable set of damage parameters was carried out on model 8. Table 4 compared the experimental data with the numerical results for burst load and remote strain at failure.

Table 4: Numerical investigation of damage parameters for X52 steel using XFEM model 8

Test/ Model	σ_{maxps} (MPa)	*Gc* N/mm	Burst load (KN)	% Diff. from test	ε0.25L%	% Diff. from test
Test 8	-	-	1842.6	-	0.2428	-
Model 8	700	500	1647.0	-10.6%	0.1927	-20%
Model 8	**700**	**900**	**1734.0**	**-6%**	**0.2125**	**-12.5%**
Model 8	700	1200	1771.0	-4%	0.2253	-7.2%
Model 8	700	1600	1799.0	-2.4%	0.2456	+1.2%
Model 8	650	900	1673.0	-9.2%	0.1768	-27.2%
Model 8	**700**	**900**	**1734.0**	**-6%**	**0.2125**	**-12.5%**
Model 8	750	900	1771.0	-4%	0.2253	-7.2%
Model 8	800	900	1824.0	-1%	0.2304	-5.1%

From Table 4, it was observed that the set with σ_{maxps} =700MPa and *Gc*=900N/mm gave a better result compared to the experimental data. The set with σ_{maxps} =700MPa, *Gc*=1200N/mm and σ_{maxps} =750MPa, *Gc*=900N/mm gave slightly closer values to the experimental result, but the pipe did not fail in these cases

instead it leads to high stress concentrations. It was observed that the values of burst load and remote strain obtained from both models were slightly lower than those obtained from the full-scale test experiments. This could be due to the modelled flaw being sharper than the machined flaw used during the full-scale test. This might have caused the crack in the model to progress faster than that of the experiment and thereby reaching the burst load earlier and generating lower strain value at failure.

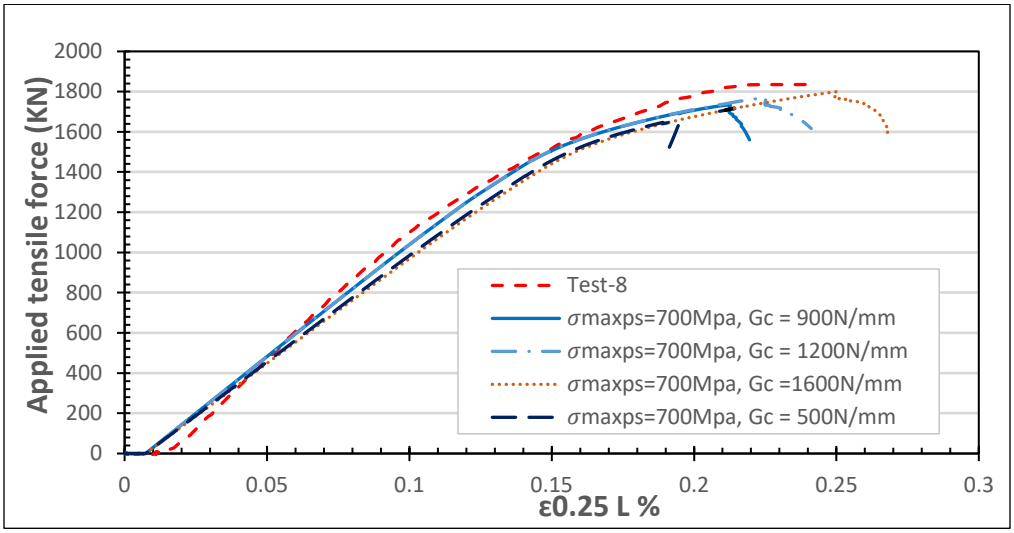

Figure 7: Applied Tensile force versus ε0.25L at constant σ_{maxps} =700MPa and varying (*Gc*) in model 8.

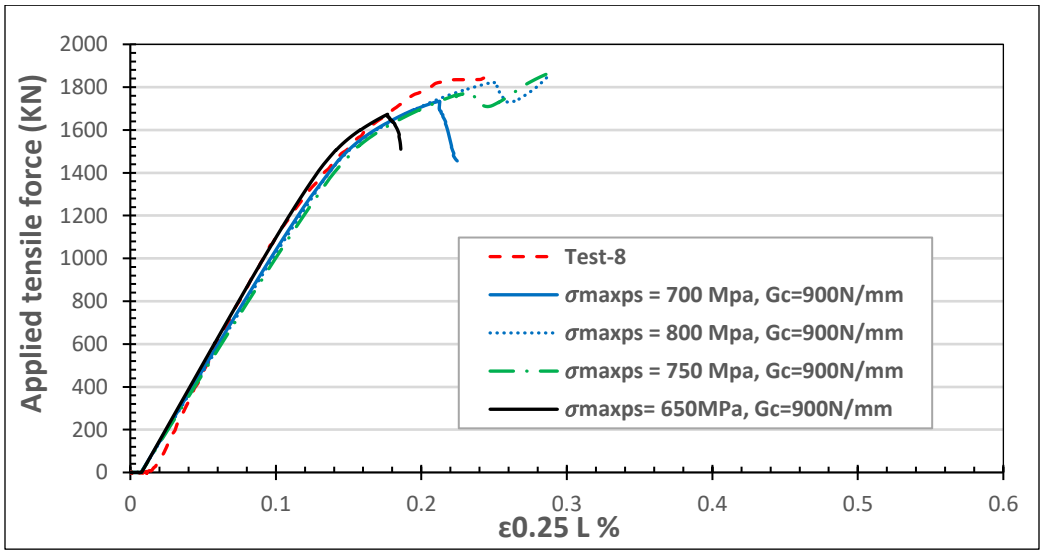

Figure 8: Applied tensile force versus ε0.25L at constant *Gc* = 900N/mm and varying σ_{maxps} in model 8.

4 Conclusion

This paper utilized the XFEM modelling technique in the prediction of burst load in pressurized NPS 12 grade X52 steel pipe. Two numerical XFEM models with the same circumferential flaw dimensions but with different levels of internal pressure were subjected to eccentric tensile loading. After some numerical investigations, σ_{maxps} of 700MPa and *Gc* of 900N/mm were identified as adequate set of damage parameters that allowed the numerical models to reproduce the experimental data with good agreement.

The result of the models showed our estimated burst load to be 1251.17KN (1302.7KN obtained from test) and remote strain as 0.15% (0.17% obtained from test) for XFEM model 7, subjected to high internal pressure of 80% SMYS. For XFEM model 8, with lower internal pressure of 30% SMYS, the burst load and remote strain increased to 1734.05KN (1843.65KN obtained from test) and 0.21% (0.24% obtained from test). The burst load and the axial remote strain of pipeline with flaw is influenced strongly by the internal pressure and that reducing the internal pressure level from 80% SMYS to 30%SMYS could increase the burst load by up to 39% and could increase the axial remote strain by about 44%.

References

Minnaar, K, Gioielli, P.C, Macia, M.L, Bardi, F, Biery, N.E and Kan, W.C. 2007. Predictive FEA Modelling of Pressurized Full-Scale Tests. International Society of Offshore and Polar Engineering, ISOPE

Wang, M. L., Horsley, D., and Zhou, J., 2006. A Quantitative Approach to Tensile Strain Capacity of Pipelines,. ASME Paper No. IPC2006-10474.

Belytschko,T and Black T. 1999. Elastic Crack Growth in Finite Elements with Minimal Remeshing. International Journal for Numerical Methods in Engineering, IJNME, 45(5): 602-620.

Moes, N, Dolbow,J. and Belytschko, T .1999. A Finite Element Method for Crack Growth without Remeshing. International Journal for Numerical Methods in Engineering, IJNME, 46(1): 131-150.

Sukumar, N, Moes, N, Moran, N and Belytschko, T. 2000. Extended Finite Element Method for Three-Dimensional Crack Modelling. International Journal for Numerical Methods in Engineering, IJNME, 48(11): 1549- 1570.

Nagashima, T, and Suemasu, H. 2010. XFEM Analyses of a Thin-Walled Composite Shell Structure with a Delamination. Computer and Structure, CS, 88(9-10): 549-557.

Zhang,B, Ye, C, liang, B, Zang, Z,and Zhi, Y. 2014. Ductile Failure Analysis and Crack behaviour of X65 Buried pipes using Extended Finite Element Method. Engineering Failure Analysis, EFA, 45: 26-40

Abdulhameed, D, Cetal, C, Lin, M, Cheng, R, Nychka, J, Sen, M and Adeeb, S. 2016. The Effect of Internal Pressure on the Tensile Strain Capacity of X52 Pipelines with Circumferential Flaws. Journal of Pressure Vessel Technology, ASME,138/06170-1

Sukumar, N, Chopp, D. L, Moës, N and Belytschko, T. 2001. Modelling Holes and Inclusions by Level sets in the Extended Finite Element Method, Computer Methods in Applied Mechanics and Engineering, CMAM, 190(46-47): 6183-2000.

Stolarska,M, Chopp, D. L, Moës, N. and Belytschko, T. 2001. Modelling Crack Growth by Level Sets in the Extended Finite Element Method. International Journal for Numerical Methods in Engineering, IJNME, 51 (8):943-960.

Abaqus 6.14, Analysis User's Manual Volume Number 2: Analysis, Dassault Simulia.

Zhang C, Cao, P, Cao, Y and Li, J .2013. Using Finite Element Software to Simulation Fracture Behavior of Three- point Bending Beam with Initial Crack, Journal of Software, JS, 8(5):1145-1150

Nonn, A., and Kalwa, C., 2012. Simulation of ductile crack propagation in high-strength pipeline steel using damage models. Proceedings of the 9thInternational Pipeline Conference, Calgary, Canada, IPC 90653.

Nonn, A., and Kalwa, C. 2013. Analysis of dynamic ductile fracture propagation in pipeline steels: A damage mechanics approach. Proceedings of the 6th International Pipeline Technology Conference, Ostend, Belgium, IPC S34-01.

Scheider, I., Nonn, A., Völling, A., Mondry, A., and Kalwa, C. 2014. A damage mechanics based evaluation of dynamic fracture resistance in gas pipelines. Procedia Materials Science. PMS. (19) 1956.

Lin, M, 2015, Characterization of Tensile and Fracture Properties of X52 Steel Pipes and Their Girth Welds, M.Sc. thesis, University of Alberta, Edmonton, AB.